NASA Technical Memorandum 107148
AIAA–96–0641

Aeroacoustics of Supersonic Elliptic Jets

Abbas Khavaran
NYMA, Inc.
Brook Park, Ohio

and

Nicholas J. Georgiadis
Lewis Research Center
Cleveland, Ohio

Prepared for the
34th Aerospace Sciences Meeting and Exhibit
sponsored by the American Institute of Aeronautics and Astronautics
Reno, Nevada, January 15–18, 1996

National Aeronautics and
Space Administration

Aeroacoustics of Supersonic Elliptic Jets

Abbas Khavaran *
NYMA, Inc., Lewis Research Group, Cleveland, OH 44135

Nicholas J. Georgiadis †
NASA Lewis Research Center, Cleveland, OH 44135

Abstract

The sound field due to a supersonic elliptic jet is studied by direct integration of the propagation equations. Aerodynamic predictions are based on numerical solution to the compressible Navier-Stokes equations in conservative law form, with a k-ϵ turbulence model. In the high frequency limit, the sound field is described by eigenrays that link the source of noise to an observer in the far-field. We assume that noise is dominated by fine-scale turbulence. Using methods derived from acoustic analogy, source correlation terms are simplified and a model is derived that relates jet noise intensity to the 7/2 power of turbulence kinetic energy. Local characteristics of the source such as its strength, time- or length-scale, and convection velocity are derived from mean flow predictions. Numerical results are compared with data for a Mach 1.5 elliptic jet as well as for a round jet. The study suggests that three-dimensional directivity of noise for jets of arbitrary geometry may be predicted with reasonable accuracy when refraction by mean flow gradients is properly accounted for.

Nomenclature

a, b	length of semi major and minor axes
a_∞	freestream sound speed
$a(\mathbf{X})$	local sound speed
$C(\mathbf{X})$	normalized sound speed
D_{eq}	area equivalent jet diameter
k	turbulent kinetic energy $= \overline{v_i v_i}/2$
$\mathbf{M}$	Mach vector
p_i	component of phase normal $\mathbf{p}$
s	arc length
T	turbulence intensity $=\overline{v_i v_i}/3$
$\mathbf{U_c}$	source convection velocity
U_j	jet exit velocity
v_i	fluctuating velocity component
ϵ	dissipation rate of kinetic energy $= \nu\overline{(\partial v_i/\partial X_j)(\partial v_i/\partial X_j)}$
θ_∞	polar observer angle
Θ	momentum thickness
ξ_1, ξ_2	elliptic coordinates
ρ	density
τ	time-delay of correlation
ϕ_∞	azimuthal observer angle
ω, Ω	observer and source frequencies

Subscripts

o	source location
∞	far field

* Senior Research Engineer, Member AIAA.
† Research Engineer, Member AIAA.

1. Introduction

Jet exhaust noise during takeoff and landing continues to be a leading environmental barrier in development of the future High-Speed Civil Transport (HSCT). Mechanical suppressors may result in unwanted engine size and performance penalty for the level of noise reduction required for HSCT certification. Fundamental aerodynamic and acoustic tests accompanied with flow and noise prediction studies are underway in the hope of advancing insight into noise generation and suppression mechanisms.

Theoretical models based on Acoustic Analogy or Linear Inviscid Instability Wave Model[1] have been successful in predicting exhaust noise for simple round nozzles under a wide range of operating conditions. In addition, new numerical algorithms tailored specifically for aeroacoustics problems are currently under development that will attempt to predict jet noise from first principles[2]. However, because of the complex issues involved, Computational Aeroacoustics (CAA) is not expected to mature into a practical engineering tool in the near future.

In the absence of shock associated noise and screech, turbulence mixing noise is considered to be the main contributor to the noise of high speed jets. At subsonic and lower supersonic speeds, small scale turbulence is regarded as the primary acoustic source. These sources are described as multipole sources that convect downstream and emit sound that may be refracted by mean flow gradients[3]. As jets becomes highly supersonic, large-scale structures or instability waves of the flow[4] become increasingly more active. In the present study, we assume that fine-scale turbulence is the source of jet noise. It is known that computation of source correlation terms

according to the Acoustic Analogy approach will require exact knowledge of the time-dependent flow fluctuations. However, it is possible to resort to simplifying assumptions, as suggested by Ribner[5] and to approximate source correlations from mean flow considerations. As such, for quasi-incompressible isotropic turbulence, the source strength will relate to the 7/2 power of turbulence kinetic energy[6]. Consequently, a full Reynolds-averaged Navier-Stokes solver with a k-ϵ turbulence model[7] will be employed to predict the mean flow and time averaged turbulence properties.

Section 2.1 describes a methodology for estimation of the source strength and turbulence scales needed to predict the spectra. In section 2.2 we focus on the high frequency geometric acoustics and sound/flow interaction of non-axisymmetric jets. A system of six propagation equations are solved numerically in a rectangular coordinate system. We map the CFD solution to a uniform grid, i.e., a grid independent of the streamwise direction, and apply a three-dimensional spline interpolation on flow parameters of interest. Mean flow gradients are computed readily from the ensuing spline coefficients as the numerical solution of refraction equations proceed along rays of geometric acoustics.

Section 2.3 presents the aerodynamic predictions and data for a shock-free Mach 1.5 aspect ratio AR=2:1 elliptic jet as well as a convergent-divergent round nozzle operating at similar conditions. Acoustic predictions are compared with data in section 2.4. Here, we examine sensitivity of the predicted zone of silence with respect to mean flow predictions. The predicted sound directivity demonstrates that noise on the major axis side is several dB's lower than the minor axis side of the elliptic jet, in good agreement with data. We discuss some shortcomings in spectral predictions that might relate to source modeling. In addition, the elliptic jet is averaged azimuthally and Balsa's[8] closed-form solution for an axisymmetric jets is applied to predict the noise. This is followed by discussions and conclusions in the final section.

2. Method of Solution

A variety of solutions based on the Analogy approach have been suggested in the literature and used with various degrees of success[5,9-12]. With a compact eddy approximation, the solution is essentially a Fourier transform of space-time correlation function, integrated over the entire jet volume. Availability of unsteady flow solutions should, in principle, make it possible to compute correlation functions of various order and orientation. Today's computational capabilities, perhaps, should encourage this effort, at least, for a selected number of source volume elements within the jet. The immediate benefit would include assessment of a number of simplifying assumptions that have traditionally been employed for source modeling. For the present work, however, we follow an approach based on separability of space-time correlation and rather focus on refraction and shielding of non-axisymmetric geometries.

2.1 Source Description

As described previously, any attempt to integrate the source correlation function over the jet volume would require modeling of these functions. Reference 6 outlines a procedure used in the present study and we briefly discuss some of the more important steps. Roughly speaking, various regions of turbulence of size ℓ, commonly referred to as an eddy volume element, radiate sound to far-field that may be summed up for all regions of the jet if the correlation volume elements radiate independently. In addition, acoustical compactness which allows for the use of elementary solutions like simple sources to model complex sources of sound such as quadrupoles requires that $\omega\ell/a_\infty$ be small. This condition requires that the *r.m.s.* velocity fluctuation be small relative to ambient sound speed[13] , i.e., $< v^2 >^{1/2}/a_\infty \ll 1$, which makes the turbulence length-scale small relative to the acoustic wave length. It should be noted that the compactness condition is not that restrictive and may hold true even at moderate Mach numbers. Assuming that noise is dominated by fine-scale turbulence, contributions from the self-noise term, in absence of refraction and convection, is shown to be due to a fourth-order space-time correlation function $\overline{v_i v_j v'_k v'_\ell}$. As is usually done, the above term is expressed as a linear combination of second-order correlations $\overline{v_i v'_j}$. This is followed by the space-time separation given as $\overline{v_i v'_j} = R_{ij}(\vec{\zeta})g(\tau)$, where $\vec{\zeta}$ and τ are the separation vector and time-delay respectively. For homogeneous isotropic turbulence, Batchelor[14] suggests a space function of the form

$$R_{ij}(\vec{\zeta}) = T[(f + \frac{1}{2}\zeta f')\delta_{ij} - \frac{1}{2}f'\zeta_i\zeta_j/\zeta]. \qquad (1)$$

Details of $f(\zeta)$ are provided in Ref. 15 and are not repeated here. A Gaussian function is normally selected for the time-factor part as $g(\tau) = exp(-\tau^2/\tau_o^2)$, with τ_o representing the characteristic time-delay of the correlation. It was shown (Ref. 6) that τ_o may be derived from the ratio of kinetic energy of turbulence k and its dissipation rate ϵ as $1/\tau_o \sim \epsilon/k$. Noise spectra due to a unit volume of turbulence, and arising from the source correlation term $\overline{v_1 v_1 v'_1 v'_1}$ may be written as

$$I_{1111}(\Omega) = \frac{3}{8\sqrt{\pi}}\rho_o^2 k^{\frac{7}{2}}(\Omega\tau_o)^4 e^{\frac{-(\Omega\tau_o)^2}{8}}. \qquad (2)$$

A Doppler factor relates source frequency Ω to the observer frequency ω. Contributions from other source correlation components $I_{ijk\ell}$ are expressed similarly[6].

2.2 Sound/Flow Interaction

In a high frequency approximation, it is normally assumed that the acoustic wave length is shorter than the characteristic length of the mean flow. For high speed jets, this approximation can be used effectively to produce the more energetic part of the sound spectra and for Helmholtz numbers (fD/a_∞) as small as one (see Tester and Morfey[15]). When a parallel flow approximation is invoked, refraction of jet noise through a sheared mean flow of arbitrary geometry may be formulated as a two-dimensional geometric acoustic problem[16]. It is argued[17] that for high speed flows, jet spreading may play a significant role in defining the size of cone of silence which is formed in the neighborhood of the downstream jet axis. In such cases, flow spreading may be accounted for by formulating a three-dimensional ray-acoustic problem. Thus, as acoustic energy, released from each finite volume of turbulence propagates out of the shear-layer, its spreading is inferred from the area of a ray-tube surrounding that ray.

For an inviscid flow governed by linearized gas dynamic equations, the coordinate $\mathbf{X}$ of the emitted sound at any point s along the ray is determined from a set of six equations[17,18]

$$\frac{dX_i}{ds} = T_{ij}p_j + M_i/C \qquad i,j = 1,2,3$$

$$\frac{dp_i}{ds} = -\frac{1}{2}p_j\frac{\partial T_{jk}}{\partial X_i}p_k - p_j\frac{\partial}{\partial X_i}(\frac{M_j}{C}) + \frac{1}{2}\frac{\partial}{\partial X_i}(C^{-2}) \quad (3a)$$

and

$$T_{ij} = \delta_{ij} - M_iM_j$$

$$\mathbf{M}(\mathbf{X}) = \frac{\mathbf{U}(\mathbf{X})}{a(\mathbf{X})}, \qquad C(\mathbf{X}) = \frac{a(\mathbf{X})}{a_\infty}. \quad (3b)$$

Vector $\mathbf{p}$ is normal to the phase front and M_i denotes the component of the Mach vector $\mathbf{M}$. Equations (3) are solved numerically subject to initial conditions associated with the source location and direction of emission. Let unit vector $\hat{\mathbf{X}} = (cos\,\mu,\ sin\,\mu\,cos\,\delta,\ sin\,\mu\,sin\,\delta)$ denote the direction of emission at the source, and subscripts o and ∞ refer to source and observer locations respectively, then

$$\mathbf{X} = \mathbf{X_o} \qquad at \quad s = 0$$

$$\mathbf{p_o} = \lambda\hat{\mathbf{X}} + (\lambda\hat{\mathbf{X}}\cdot\mathbf{M} - \frac{1}{C})\frac{\mathbf{M}}{\beta^2}, \quad (4a)$$

where

$$\lambda = [\beta^2 + (\hat{\mathbf{X}}\cdot\mathbf{M})^2]^{-\frac{1}{2}}/C \quad (4b)$$

$$\beta^2 = 1 - |\,\mathbf{M}\,|^2.$$

As rays emerge from the shear layer, they become straight and the ray speed λ approches one. For every set of radiation angles (μ, δ) a pair of angles (θ_∞, ϕ_∞) may be calculated from equations (3). Variation of the ray-tube area is then expressed as the Jacobian of the transformation, i.e., $|\,\partial(\theta_\infty, \phi_\infty)/\partial(\mu, \delta)\,|$. It is shown[17,19] that the far-field mean square pressure directivity for a convecting quadrupole source of strength $Q_{ij}(\Omega)$ becomes

$$\overline{P^2_{Q_{ij}}} \propto (\frac{\rho_\infty a_\infty}{4\pi R})^2\Omega^4(\frac{Q_{ij}p_ip_j}{|\,\mathbf{p}\,|^2})^2_o(\frac{a_o^2}{a_\infty^2}\frac{\lambda_o^3}{\rho_o})\times$$

$$\frac{(1-\frac{\mathbf{U_o}}{a_\infty}\cdot\mathbf{p_o})^2(1-\frac{\mathbf{U_\infty}}{a_\infty}\cdot\mathbf{p_\infty})^2}{(1-\frac{\mathbf{U_c}}{a_\infty}\cdot\mathbf{p_o})^5}(\frac{sin\,\mu}{sin\,\theta_\infty}\frac{1}{|\,\frac{\partial(\theta_\infty,\phi_\infty)}{\partial(\mu,\delta)}\,|}) \quad (5)$$

where $\mathbf{U_c}$ is the source convection velocity and ω is the observer frequency related to source frequency Ω as

$$\omega = \Omega/(1 - \frac{\mathbf{U_c}}{a_\infty}\cdot\mathbf{p_o}). \quad (6)$$

For an isotropic quadrupole source, $Q_{ij}p_ip_j = Q_o\,|\,\mathbf{p}\,|^2$. If source spectral power density Q_o^2 is replaced with I_{1111}/Ω^4 from (2), the directivity pattern is found as

$$\overline{P^2_{Q_o}} \propto (\frac{a_\infty}{4\pi R})^2(\rho_\infty^2k^{\frac{7}{2}})(\Omega\tau_o)^4e^{\frac{-(\Omega\tau_o)^2}{8}}(\frac{a_o^2}{a_\infty^2}\lambda_o^3\rho_o)\times$$

$$\frac{(1-\frac{\mathbf{U_o}}{a_\infty}\cdot\mathbf{p_o})^2(1-\frac{\mathbf{U_\infty}}{a_\infty}\cdot\mathbf{p_\infty})^2}{(1-\frac{\mathbf{U_c}}{a_\infty}\cdot\mathbf{p_o})^5}(\frac{sin\,\mu}{sin\,\theta_\infty}\frac{1}{|\,\frac{\partial(\theta_\infty,\phi_\infty)}{\partial(\mu,\delta)}\,|}). \quad (7)$$

Roughly speaking, when the difference between $\mathbf{U_o}$ and $\mathbf{U_c}$ is small, and assuming that $\mathbf{U_\infty}$ is negligible, the directivity pattern scales as $(1-\frac{\mathbf{U_c}}{a_\infty}\cdot\mathbf{p_o})^{-3}$ outside the zone of silence. Near and within the boundary of zone of relative silence, the factor $(\frac{sin\,\mu}{sin\,\theta_\infty})/|\,\partial(\theta_\infty, \phi_\infty)/\partial(\mu, \delta)\,|$ alters the above directivity and results in concentration of noise near the boundary of zone of silence, i.e., a sharp peak followed by a rapid decay into the zone of silence.

2.3 Aerodynamic Predictions

Flow predictions were made with the NPARC Navier-Stokes code and with a recently installed[20] low Reynolds number k-ϵ model of Chien[21]. The conical and elliptic jets considered had an exit area of 1.571 in^2 each, with aspect ratio of AR=2:1 for the elliptic jet. Both nozzles are operated at the design pressure ratio of 3.67 and 564° R total temperature to give exit Mach number of 1.5. Some aerodynamic and acoustic data[22] were available for validation. Because of symmetry, only one quarter of the elliptic jet is modeled. The major and minor axes are planes of symmetry modeled with NPARC's slip wall boundary conditions. A grid having 121×91 points in axial and radial directions and 25 points in circumferential direction was selected. The domain of the

grid includes 10 diameters into the nozzle and up to 70 diameters downstream of the exit plane.

It is convenient to introduce elliptic coordinates ξ_1 and ξ_2 with

$$y = \xi_1 cos\,\xi_2, \qquad z = (\xi_1/p)\,sin\,\xi_2, \qquad x = x, \qquad (8)$$

where x is the streamwise direction. The above coordinates maintain a constant aspect ratio of $p = a/b$, with an area element $dA = (\xi_1/p)d\xi_1 d\xi_2$ (see figure 1a). Within one quarter of the elliptic jet, the azimuthal angle ϕ, measured from the major axis, is equally divided over 25 grid points and relates to elliptic angle ξ_2 as $tan\,\xi_2 = p\,tan\,\phi$. Two-dimensional views of the elliptic grid for major axis plane xy and spanwise plane yz are shown in figures 1b and 1c.

Compressible flow solvers like NPARC have difficulty converging slow flow or stagnant air regions. To help convergence, the surrounding air (at rest in experiment) was set to an inflow total pressure that provides a 0.1 ambient Mach number. With a slip-type boundary condition for the surrounding flow, the predicted centerline velocity decay is shown in figure 2a. In the experiment, centerline velocity was supersonic out to $14.2D$ for conical flow and to $11.2D_{eq}$ for the elliptic jet, indicating several diameters reduction in the supersonic core-length from round to elliptic nozzle. The NPARC kϵ prediction with the above boundary condition (referred to as solution-A hereafter) gives supersonic core length of $13.3D$ and $12.7D_{eq}$ respectively. A second pair of solutions (solution-B) was obtained by extending the grid farther out in the spanwise direction and using a free-type boundary for the surrounding flow. Here, the ambient Mach number may be reduced to zero without convergence difficulties. The new centerline velocity decay (figure 2b) gives supersonic core lengths of $11.9D$ and $11.3D_{eq}$ for round and elliptic jets. Although the elliptic jet appears to show improved agreement with data, the difference in supersonic core length between the two nozzles is still not as dramatic as the data indicate. The aeroacoustic predictions that follow are based on solution-B, unless specified otherwise.

Velocity profiles along the major and minor axes of the elliptic jet are shown in figures 3a and 3b respectively. Comparison with data of Seiner[22] demonstrates good agreement along the minor axis plane. However, the major axis predictions appear to underestimate the spreading rate. A similar conclusion may be drawn from the axial distribution of momentum thickness defined for compressible flows

$$\Theta = \int_0^\infty \frac{\rho U}{(\rho U)_{cl}}(1 - \frac{U}{U_{cl}})dr, \qquad (9)$$

where subscript cl denotes the centerline values. The predicted momentum thickness (figure 4a) shows little difference along the major and minor axes near the exit. A more pronounced difference is observed downstream where thickness along the major axis shows a slightly faster growth rate. The round nozzle momentum thickness in figure 4a is in agreement with the elliptic jet's minor axis. Data of figure 4b indicates that momentum thickness is nearly equal along both axes over the length of the potential core and starts to grow at a faster rate along the major axis near the end of the core. Notice that the round nozzle momentum thickness, shown here for a design Mach number of 2.0, is in agreement with the general behavior along the minor axis as was concluded from predictions of figure 4a.

The initial distribution of momentum thickness has been used in the past[23,24] as a length-scale for the initial turbulent shear layer. The strength of shed vorticity around the periphery of the nozzle has been linked to the azimuthal variation of momentum thickness. According to figure 4b, distortion of the jet column starts near the end of the core and there is little distortion within the core. In linear inviscid stability analysis of supersonic elliptic jets[25,26], it is argued that the lowest order azimuthal mode, commonly referred to as varicose or axisymmetric mode, governs the stability of a shock-free supersonic jet. This mode is believed to reach maximum amplification near the axial location where the rapid growth of major axis momentum thickness occurs, and decays thereafter.

Turbulence intensity profiles along major and minor axes of the elliptic jet are shown in figures 5a and 5b. Here the percent turbulence is defined as $100 \times (v_i v_i/3)^{1/2}/U_j$. Both figures indicate a maximum level in the neighborhood of the jet lip-line and an exit value of 11.3%, that will gradually increase to 12.5% at about $5D_{eq}$ and decays farther downstream. The centerline value is zero within the core to about $6D_{eq}$ and will rise to 3.4% at $7.3D_{eq}$ and 8.7% at $10.7D_{eq}$. Although the existing modifications[20] in NPARC allow for turbulence kinetic energy input as an inflow boundary condition, the predictions within the core remain insensitive to the specified inflow values. Experiments should be performed to verify turbulence predictions.

2.4 Acoustic Predictions

Computation of sound pressure level directivity (SPL) and spectra is carried out according to equation (7). At each finite volume of turbulence ΔV, the source strength $k^{7/2}$ and characteristic time-scale τ_o are derived from the NPARC kϵ solutions according to $1/\tau_o = \alpha(\epsilon/k)$. Constant α is selected empirically and source convection velocity $\mathbf{U_c}$ is expressed as weighted average

of exit and local velocities $\mathbf{U_c} = 0.5\mathbf{U_o} + 0.3\mathbf{U_j}$. For an observer frequency ω , the corresponding source frequency Ω is calculated from equation (6), where $\mathbf{p_o}$ denotes the normal to the phase front at the source. At selected observer coordinates (R, θ_∞, ϕ_∞), the source radiation angles (μ, δ) and the corresponding phase normal $\mathbf{p_o}$ are found by solving (3) and (4) numerically as a boundary-value problem. Once the missing initial values are found, they may be used as a first guess for the neighboring source volume element and the process continues.

In order to integrate the propagation equations, a B-spline interpolation of the CFD solutions is carried out in three dimensions

$$\sum_{\ell=1}^{N_{\xi_2}} \sum_{m=1}^{N_{\xi_1}} \sum_{n=1}^{N_x} C_{nm\ell}\, B_{n,k_x,t_x}(x)\, B_{m,k_{\xi_1},t_{\xi_1}}(\xi_1) \times$$

$$B_{\ell,k_{\xi_2},t_{\xi_2}}(\xi_2) = f(x,\xi_1,\xi_2). \qquad (10)$$

Tensor coefficients $C_{nm\ell}$ may be found for each flow parameter of interest by solving (10) as a system of simultaneous equations applied to data points (x, ξ_1, ξ_2, f). Here k_x, k_{ξ_1} and k_{ξ_2} are the orders of spline , t_x, t_{ξ_1} and t_{ξ_2} are the corresponding knot sequence in x, ξ_1 and ξ_2 directions respectively[27], and $B_{n,k,t}$ denotes the n-th B-spline of order k with respect to knot sequence t. It should be noted that the above process assumes a uniform grid, i.e., one independent of the streamwise direction. To this end, a postprocessing of the CFD solution may be necessary. This is usually done by selecting a common spanwise grid structure, say one defined at $X/D_{eq} = 10.0$, and consequently mapping the flow field to this grid at each streamwise location using a two-dimensional B-spline interpolation. Once spline coefficients $C_{nm\ell}$ in equation (10) are determined, the directional derivatives become readily available at any point within the jet.

It is known that refraction results in a zone of silence for the high frequency noise. The zone of silence, denoted as $\theta^*(\mathbf{X_o})$, and measured from the jet axis, is defined as the smallest polar angle that may receive acoustic signal from a source. This angle is found at each source location $\mathbf{X_o}$ by solving equations (3) subjet to initial conditions $(\mu, \delta) = (0, 0)$. Obviously, for off-axis sources, a complete refraction may be achieved with a small value of cone angle μ if δ is such that sound is directed towards the centerline. This may explain the observed smooth transition of SPL directivity into the zone of silence. However, the peak directivity level for a selected source is in the very neighborhood of θ^*.

Figure 6a shows the boundary of zone of silence for sources located on the major axis plane, x-y, of the elliptic jet. The source axial location is indicated as the parameter X_o/D_{eq}. It is clearly seen that for the most part, more energetic segments of the jet, i.e. sources near the lip-line $Y_o/a = 1.0$, radiate primarily in direction of $\theta^* = 50°$. This is consistent with the reported directivity for the high Strouhal number noise for Mach 1.5 elliptic jet. The effect of the ambient Mach number $M_\infty = 0.1$ on the refraction angles is shown in figure 6b as a reduction in shear and hence a reduction in refraction angle by nearly 8 degrees. The corresponding SPL directivity is expected to show a similar shift in angle relative to the static case. Sensitivity of the zone of silence with respect to azimuthal source location is shown in figure 7. Generally speaking, the flow asymmetry will result in an increase in the size of cone of silence as the source moves azimuthally closer the minor axis.

As a first approximation, the elliptic jet was mass-averaged azimuthally. Predictions are on a 12 foot sideline. The sound pressure level directivity for an equivalent axisymmetric jet as well as a Mach 1.5 conical jet are shown in figure 8a. Here, the high frequency solution to Lilley's equation in cylindrical coordinates combined with a parallel flow assumption[8] is used to assess the sound/flow interaction. For non-axisymmetric flows, azimuthal measurements normally show lower noise on the deep side of a jet, such as the major axis of the elliptic jet. In addition, the jet asymmetry will usually result in enhanced mixing and help decay the core velocity and therefore reduce noise. Our numerical prediction did not indicate a significant increase in centerline velocity decay as discussed earlier in figure 2b. However, the predictions of figure 8b appear to shows favorable agreement with data. This is conceivably the result of artificial mixing that is achieved by circumferential averaging of the flow. No data was available for the conical nozzle at this point, however, based on data reported at higher temperatures[28], it is anticipated that the conical nozzle is at least as noisy as the minor axis side of the elliptic jet. Shown in figure 9a are the spectral measurements along the major axis plane of the elliptic jet. Generally speaking, data indicate a shift in spectral peak to higher frequencies with increasing polar angle θ_∞. Predicted spectra based on high frequency solution to Lilley's equation (figure 9b), however, do not seem to follow a similar trend. It is conjectured that this may be associated with simplistic replacement of the fourth-order space-time correlation functions.

To assess the general directivity, a matrix of five polar angles $\theta_\infty = 50°$ to $110°$, in increments of $15°$, and four azimuthal angles $\phi_\infty = 0°$ to $90°$, increments of $30°$ is selected. The spherical directivity of noise for this elliptic jet as predicted with a 3DGA approach is shown in figure 10a. Azimuthal directivity, for the most part, shows 2 dB lower noise on the major axis side, in good agreement with data of figure 8b. Predicted zone of silence, however, appears larger than measurements. This

is primarily due to the absence of low frequency noise in the present calculations, which is known to make a significant contribution near the jet axis. In addition, an accurate prediction of the mean flow profiles can have a significant bearing on refraction angles. This was illustrated earlier when comparing figures 6a and 6b. Had we selected solution-B (with $M_\infty = 0.1$), the cone of silence would have been smaller by 8 degrees. The spectral distribution, figure 10b, shows relatively small low frequency content. This is an indications of the failure of the present approach when it is pushed to the low frequency limit. Low frequency sound from moving multipole sources in axisymmetric shear flows (see Ref. 29) may be extended to arbitrary geometries to produce the lower end of the spectra. The predicted shift in spectra with polar observer angle remains consistent with earlier prediction for the equivalent axisymmetric jet, and using Balsa's approach. This may again confirm our stipulation on the need for an improved source modeling.

Finally, in figure 11 we demonstrate the spherical directivity for a typical elliptic ring source along the lipline, i.e., $\xi_1/a = 1$, and at $X/D_{eq} = 6.3$. Selected source location corresponds to a region of relative high turbulence. This figure suggests that the basic azimuthal pattern of jet noise may be captured readily by selection of appropriate source elements within acoustically active regions of the flow and without a need for complete volume integration.

3. Concluding Remarks

The present paper provides a methodology for the prediction of noise from noncircular jets. The calculations employ a full 3D geometric acoustic approach to assess the spherical directivity of noise from a shock-free turbulent jet. Predictions assume that noise is generated by small scales of motion and is dominated by the high end of the spectra. Other approaches need to be combined with the ray-acoustics in order to predict the lower end of the spectra. Accurate prediction of the mean flow parameters, such as the jet spreading, centerline velocity decay, turbulence level and its dissipation rate are the first step requirements for the present noise predictions. Contributions from large-scale coherent structures may be accounted for via a linear inviscid stability analysis. Stability type analysis, however, is highly geometry dependent and has been fully explored in Ref. 26 for an elliptic geometry assuming a simple representation of the mean velocity profiles.

As discussed, a revisit of the turbulence correlation function for the purpose of source modeling and validation is appropriate at this point. Despite this needed improvement, ray acoustic approach as presented here, sheds light on the importance of the mean flow interaction and the role it plays in shaping the directivity of jet noise.

4. Acknowledgements

This work was supported by NASA Lewis Research Contract NAS3-27186. The technical monitor was E. A. Krejsa. The authors are also grateful to Dr. J.M. Seiner for supplying the experimental data.

References

[1]Tam, C. K. W. and Burton, D.E., "Sound Generated by Instability Waves of Supersonic Flows. Part 2. Axisymmetric Jets," *J. Fluid Mech.*, **138**, 1984, pp. 273-295.

[2]Tam, C. K. W., "Computational Aeroacoustics: Issues and Methods," AIAA Paper 95-0677, 1995.

[3]Ribner, H. S., "An Extension of the Lighthill Theory of Jet Noise to Encompass Refraction and Shielding," NASA TM-110163, 1995.

[4]Tam, C. K. W., "Aerodynamics of Flight Vehicles: Theory and Practice," NASA Ref. Pub. 1258, Vol. 1, 1991, pp. 311-390.

[5]Ribner, H. S., "Quadrupole Corrections Governing the Pattern of Jet Noise," *J. Fluid Mech.*, **38**, 1969, pp. 1-24.

[6]Khavaran, A., Krejsa, E. A., and Kim, C. M., "Computation of Supersonic Jet Mixing Noise for an Axisymmetric Convergent-Divergent Nozzle," *AIAA J. Aircraft*, **31**, 1994, pp. 603-609.

[7]Cooper, G. K. and Sirbaugh, J. R., "PARC Code: Theory and Usage", Arnold Engineering Development Center Report AEDC-TR-89-15, 1989.

[8]Balsa, T. F., "The Far Field of High Frequency Convected Singularities in Sheared Flows, with an Application to Jet Noise Prediction," *J. Fluid Mech.*, **74**, 1976, pp. 193-208.

[9]Ribner, H. S., "On the Role of Shear Term in Jet Noise," *J. Sound Vib.*, **52(1)**, 1977, pp. 121-132.

[10]Chu, W. T., "Turbulence Measurement Relevant to Jet Noise," Univ. of Toronto, Institute for Aerospace Studies, UTIAS Rept. 119, 1966.

[11]Chu, W. T., "Moving Frame Analysis of Jet Noise," *J. Acous. Soc. Am.*, **53(5)**, 1973, pp. 1439-1440.

[12]Krishnappa, G. and Casanady, G. T. " An Experimental Investigation of the Composition of Jet Noise," *J. Fluid Mech.*, **37**, 1969, pp. 149-159.

[13]Lighthill, M. J., "Jet Noise. The Wright Brothers' Lecture," *AIAA Journal.*, **1**, 1963, pp. 1507-1517.

[14]Batchelor, G. K. *The theory of Homogeneous Turbulence*, Cambridge Univ. Press, 1953.

[15]Tester, B. J. and Morfey, C. L., "Developments in Jet Noise Modeling - Theoretical Predictions and Comparisons with Measured Data," *J. Sound Vib.*, **46(1)**, 1976, pp. 79-103.

[16]Goldstein, M. E., "High Frequency Sound Emission from Moving Point Multipole Sources Embedded in Arbitrary Transversely Sheared Mean Flows," *J. Sound Vib.*,**80(4)**, 1982, pp. 499-522.

[17]Khavaran, A., Krejsa, E. A., "Refraction of High Frequency Jet Noise in an Arbitrary Jet Flow," AIAA Paper 94-0139, 1994.

[18]Durbin, P. A., "High Frequency Green Function for Aerodynamic Noise in Moving Media, part I: General Theory," *J. Sound Vib.*, **91(4)**, 1983, pp. 519-525.

[19]Durbin, P. A., "High Frequency Green Function for Aerodynamic Noise in Moving Media, part II: Noise from a Spreading Jet," *J. Sound Vib.*, **91(4)**, 1983, pp. 527-538.

[20]Georgiadis, N. J., Chitsomboon, T., and Zhu, J. "Modification of the Two-Equation Turbulence Model in NPARC to a Chien Low Reynolds Number k-ϵ Formulation," NASA TM-106710, 1994.

[21]Chien, K. Y., "Prediction of Channel and Boundary Layer Flows with a Low Reynolds-Number Turbulence Model," *AIAA Journal*, **20(1)**, 1982, pp. 33-38.

[22]Seiner, J.M., "Fluid dynamics and Noise Emission Associated with Supersonic Jets," Studies in Turbulence, edited by T.B.Getski, S. Sarkar and G. Speziale, *Springer-Verlag*, New York, 1992, pp. 297-323.

[23]Ho, C. M. and Gutmark, E., "Vortex Induction and Mass Entrainment in a Small Aspect Ratio Elliptic Jet," *J. Fluid Mech.*, **179**, 1987, pp. 383-405.

[24]Bridges, J.E. and Hussain, A.K.M.F., "Roles of Initial Condition and Vortex Pairing," *J. Sound Vib.*, **117**, part 2., 1987, pp. 289-311.

[25]Baty, R. S., Seiner, J. M., Ponton, M. K., "Instability of a Supersonic Shock-Free Elliptic Jet," AIAA Paper 90-3959, 1990.

[26]Morris, P. J., and Bhat, T. R. S., "The Prediction of Noise Radiation from Supersonic Elliptic Jets," AGARD 78th Specialist Meeting on Combat Aircraft Noise, Bonn, Germany, Oct. 1991.

[27]de Boor, C., *A Practical Guide to Splines, Springer-Verlag*, New York, 1978

[28]Seiner, J. M., and Ponton, M. K., "Supersonic Acoustic Source Mechanisms for Free Jets of Various Geometries," AGARD 78th Specialist Meeting on Combat Aircraft Noise, Bonn, Germany, Oct. 1991.

[29]Goldstein, M. E., "The Low Frequency Sound from Multipole Sources in Axisymmetric Shear Flows, with Application to Jet Noise," *J. Fluid Mech.*, **70**, 1975, pp. 595-604.

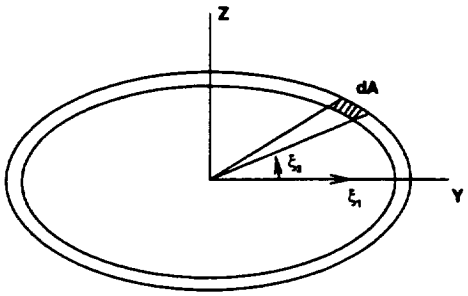

Figure 1a. Elliptic coordinates

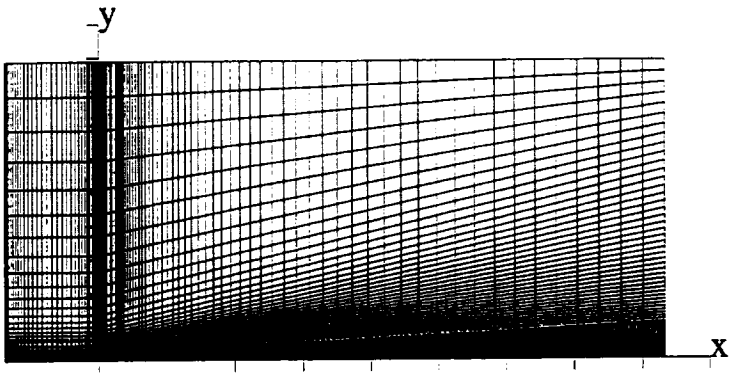

Figure 1b. Grid in major axis plane, jet exit is at X=0.0.

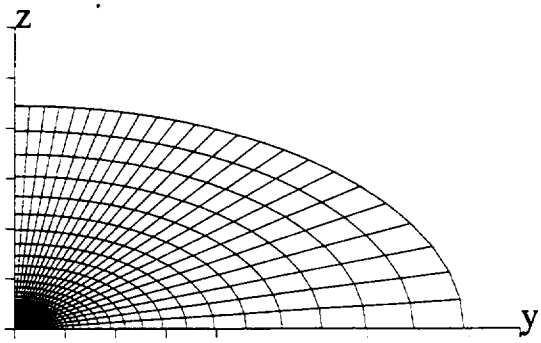

Figure 1c. Grid in a spanwise plane at X/D_{eq}=5.4.

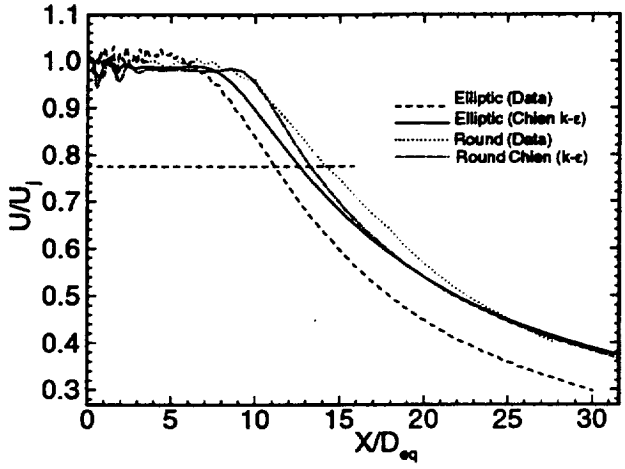

Figure 2a. Centerline velocity decay for the elliptic jet and the equivalent M=1.5 round jet. M_{-}=0.1, (solution A).

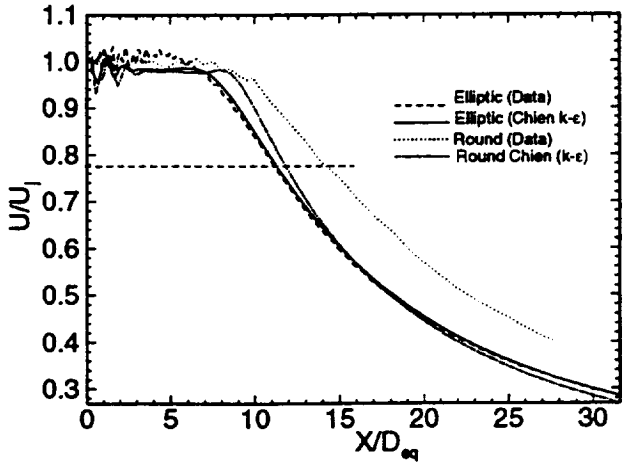

Figure 2b. Centerline velocity decay for the elliptic jet and the equivalent M=1.5 round jet. M_{-}=0.0, (solution B).

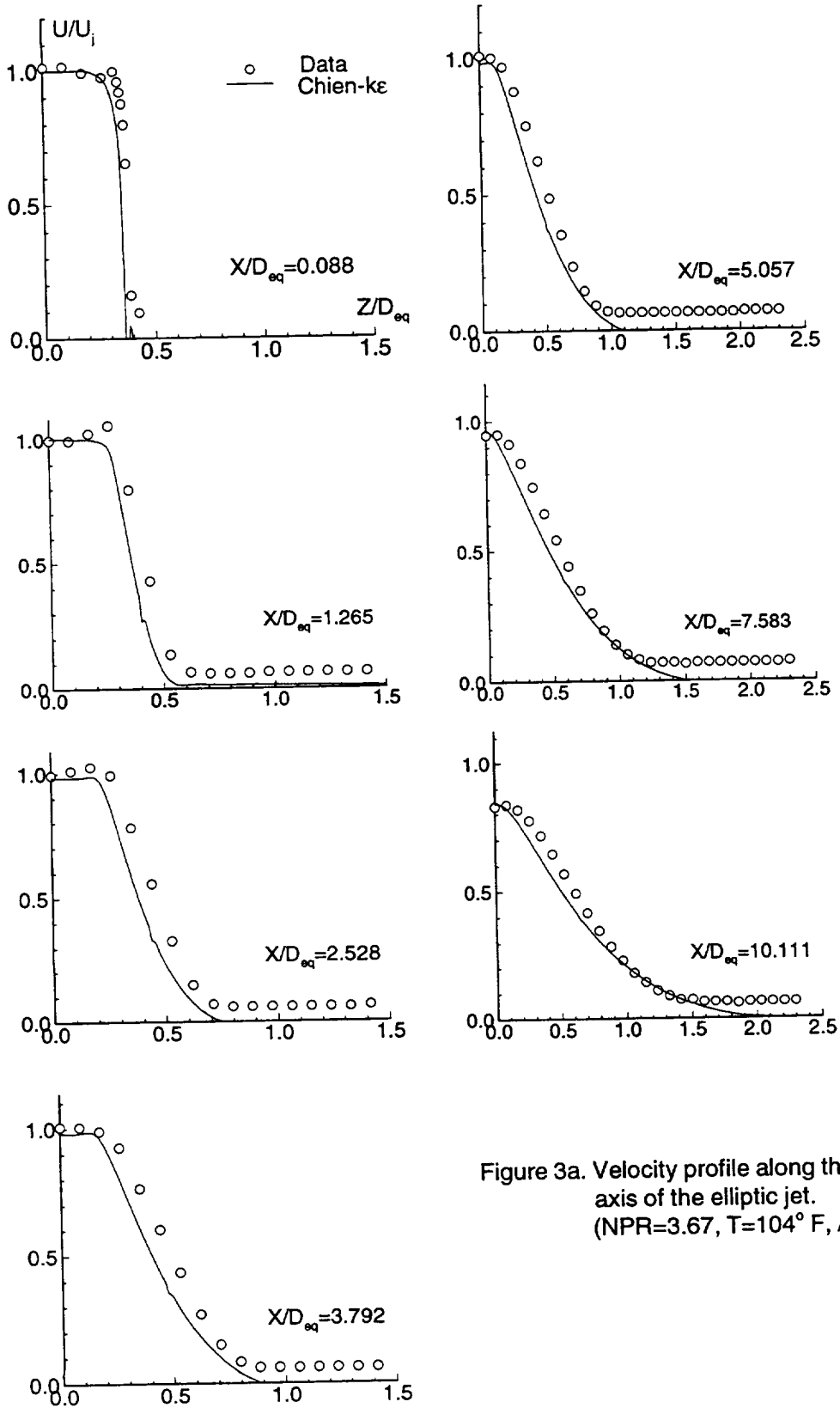

Figure 3a. Velocity profile along the minor axis of the elliptic jet. (NPR=3.67, T=104° F, AR=2:1)

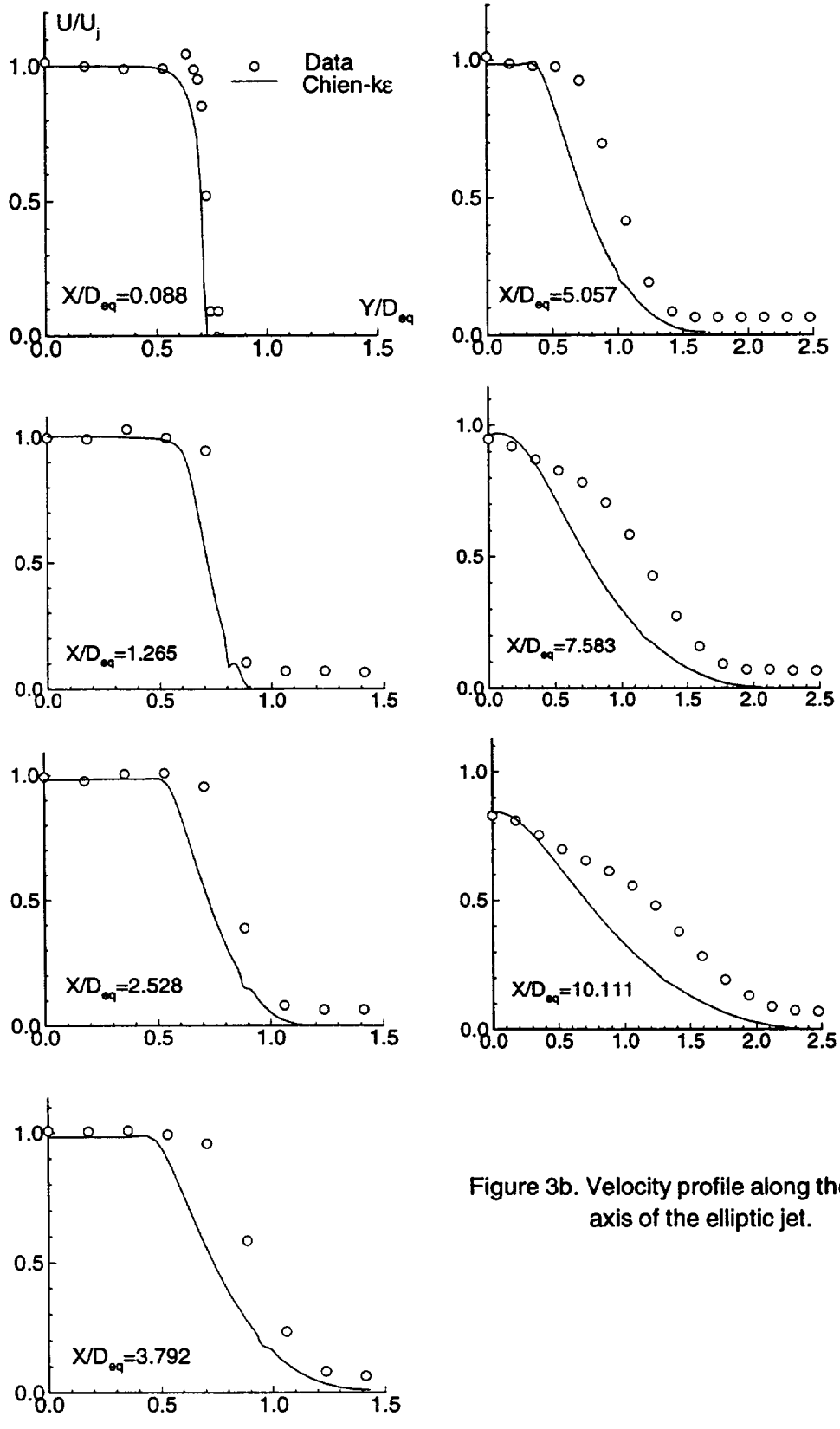

Figure 3b. Velocity profile along the major axis of the elliptic jet.

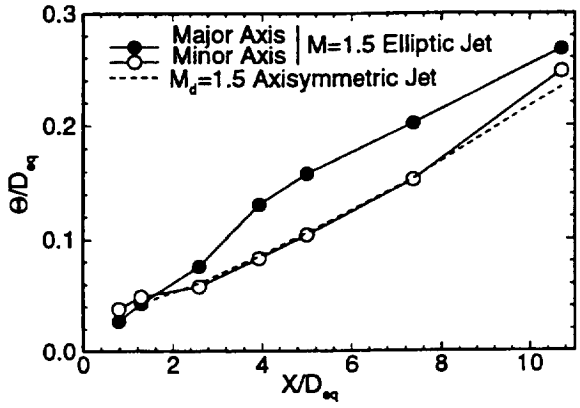

Figure 4a. Momentum thickness for round and elliptic jets (NPARC-kε).

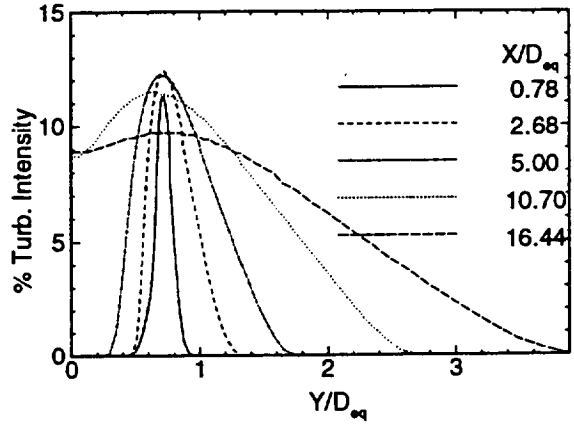

Figure 5a. Turbulence intensity along the major axis of the M=1.5 elliptic jet.

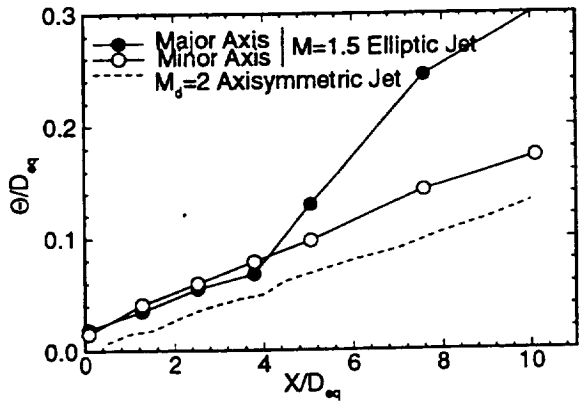

Figure 4b. Momentum thickness for round and elliptic jets (Data of Ref. 22).

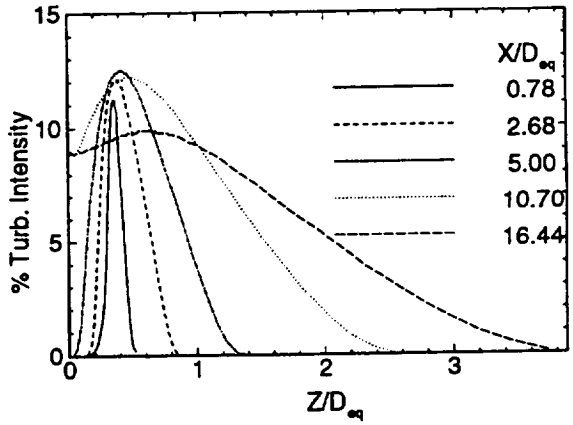

Figure 5b. Turbulence intensity along the minor axis of the M=1.5 elliptic jet.

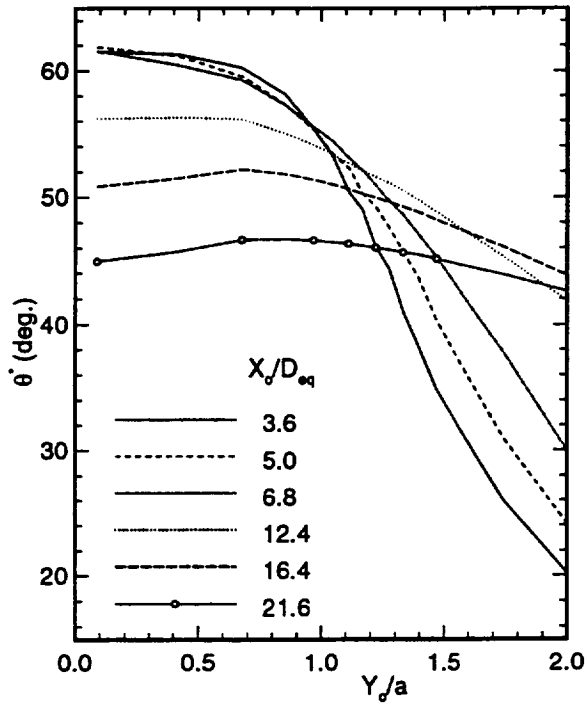

Figure 6a. Boundary of zone of silence vs. source location, Mach 1.5 (M_j=0.0) elliptic jet.

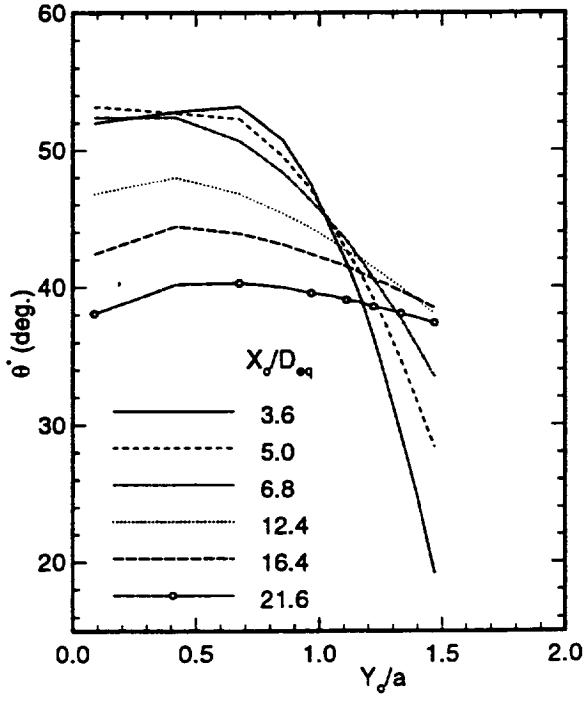

Figure 6b. Boundary of zone of silence vs. source location, Mach 1.5 (M_j=0.1) elliptic jet.

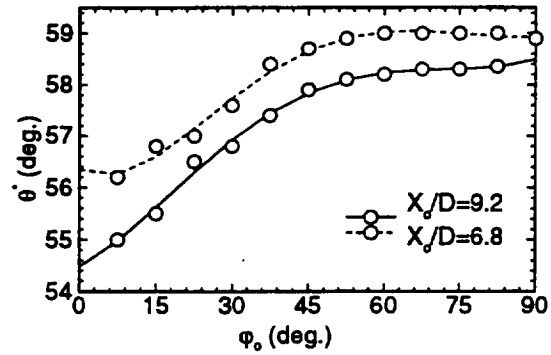

Figure 7. Boundary of the zone of silence vs. azimuthal source location. Source on an ellipse at ξ_1/a=1.0.

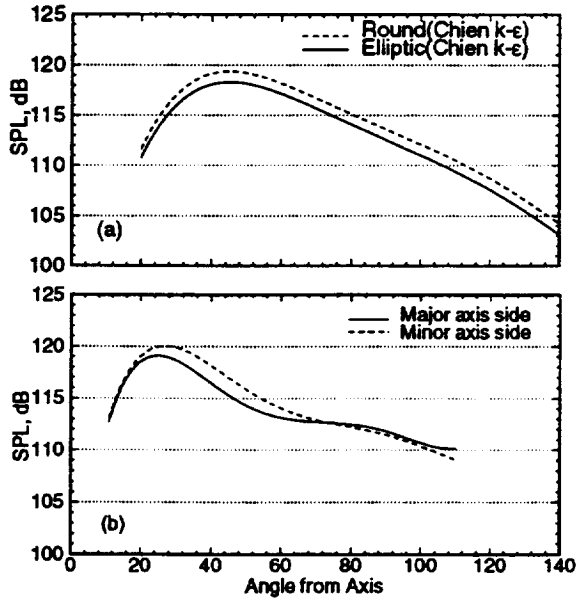

Figure 8. Sound pressure level directivity: (a) predictions for conical jet and axisymmetric equivalent to elliptic jet; (b) data for elliptic jet.

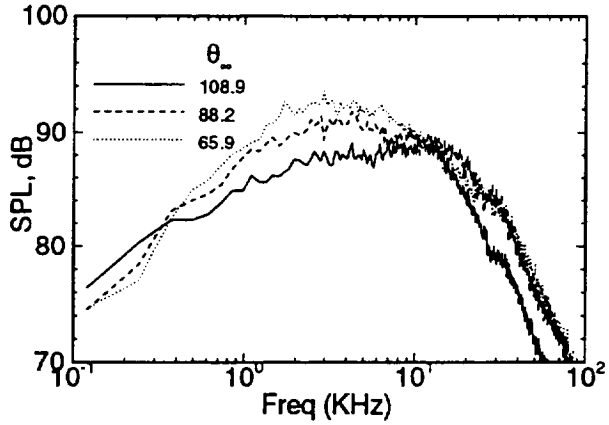

Figure 9a. Spectra at φ_{-}=0.0 for Mach 1.5, AR=2:1 elliptic jet (data).

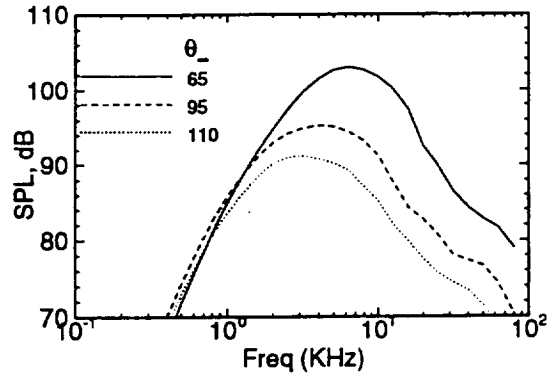

Figure 10b. Spectra at φ_{-}=0.0 for Mach 1.5, AR=2:1 elliptic jet; HFGA predictions.

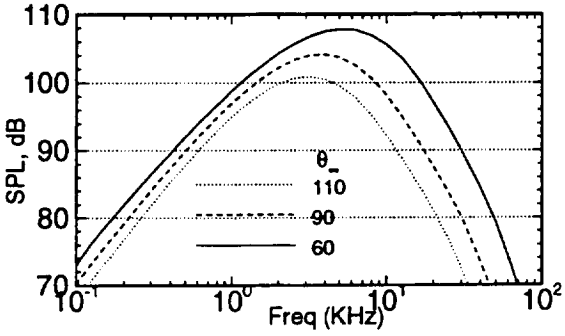

Figure 9b. Spectra (prediction) for axisymmetric equivalent to elliptic jet (Mach 1.5, AR=2:1).

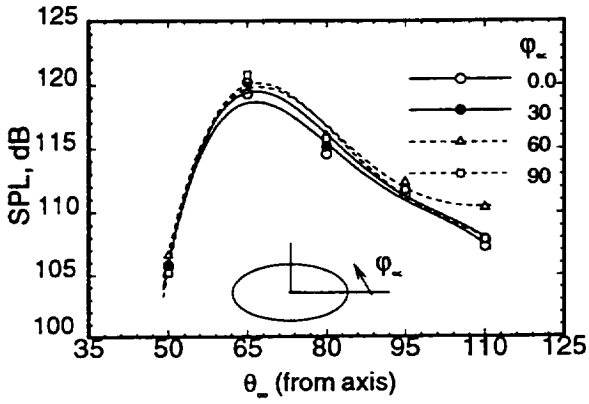

Figure 10a. Predicted SPL directivity for Mach 1.5 elliptic jet.

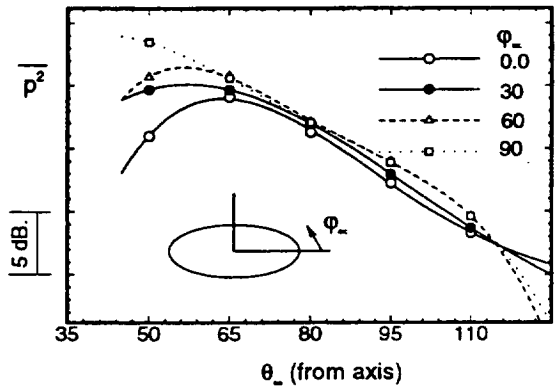

Figure 11. Predicted SPL directivity for a typical ring source within Mach 1.5 (M_{-}=0.1) elliptic jet.

REPORT DOCUMENTATION PAGE

Form Approved
OMB No. 0704-0188

1. AGENCY USE ONLY (*Leave blank*)	2. REPORT DATE	3. REPORT TYPE AND DATES COVERED
	January 1996	Technical Memorandum

4. TITLE AND SUBTITLE

Aeroacoustics of Supersonic Elliptic Jets

5. FUNDING NUMBERS

WU-538-03-11

6. AUTHOR(S)

Abbas Khavaran and Nicholas J. Georgiadis

7. PERFORMING ORGANIZATION NAME(S) AND ADDRESS(ES)

National Aeronautics and Space Administration
Lewis Research Center
Cleveland, Ohio 44135-3191

8. PERFORMING ORGANIZATION REPORT NUMBER

E-10081

9. SPONSORING/MONITORING AGENCY NAME(S) AND ADDRESS(ES)

National Aeronautics and Space Administration
Washington, D.C. 20546-0001

10. SPONSORING/MONITORING AGENCY REPORT NUMBER

NASA TM-107148
AIAA-96-0641

11. SUPPLEMENTARY NOTES

Prepared for the 34th Aerospace Sciences Meeting and Exhibit sponsored by the American Institute of Aeronautics and Astronautics, Reno, Nevada, January 15-18, 1996. Abbas Khavaran, NYMA, Inc., 2001 Aerospace Parkway, Brook Park, Ohio 44142 (work funded by NASA Contract NAS3-27186); and Nicholas J. Georgiadis, NASA Lewis Research Center. Responsible person, Nicholas J. Georgiadis, organization code 2740, (216) 433-3958.

12a. DISTRIBUTION/AVAILABILITY STATEMENT

Unclassified - Unlimited
Subject Category 71

This publication is available from the NASA Center for Aerospace Information, (301) 621-0390.

12b. DISTRIBUTION CODE

13. ABSTRACT (*Maximum 200 words*)

The sound field due to a supersonic elliptic jet is studied by direct integration of the propagation equations. Aerodynamic predictions are based on numerical solution to the compressible Navier-Stokes equations in conservative law form, with a k-ε turbulence model. In the high frequency limit, the sound field is described by eigenrays that link the source of noise to an observer in the far-field. We assume that noise is dominated by fine-scale turbulence. Using methods derived from acoustic analogy, source correlation terms are simplified and a model is derived that relates jet noise intensity to the 7/2 power of turbulence kinetic energy. Local characteristics of the source such as its strength, time- or length-scale, and convection velocity are derived from mean flow predictions. Numerical results are compared with data for a Mach 1.5 elliptic jet as well as for a round jet. The study suggests that three-dimensional directivity of noise for jets of arbitrary geometry may be predicted with reasonable accuracy when refraction by mean flow gradients is properly accounted for.

14. SUBJECT TERMS

Aeroacoustics; Jet noise; Aerodynamic noise

15. NUMBER OF PAGES

15

16. PRICE CODE

A03

17. SECURITY CLASSIFICATION OF REPORT	18. SECURITY CLASSIFICATION OF THIS PAGE	19. SECURITY CLASSIFICATION OF ABSTRACT	20. LIMITATION OF ABSTRACT
Unclassified	Unclassified	Unclassified	

National Aeronautics and
Space Administration

Lewis Research Center
21000 Brookpark Rd.
Cleveland, OH 44135-3191